ELSEVIER

Wave Motion 21 (1995) 47–66

WAVE MOTION

Numerical modeling of elastic wave propagation and scattering with EFIT – elastodynamic finite integration technique

P. Fellinger, R. Marklein, K.J. Langenberg *, S. Klaholz,

Department Electrical Engineering, University of Kassel, D-34109 Kassel, Germany

Abstract

The basic equations of EFIT, the Elastodynamic Finite Integration Technique, are formulated for anisotropic inhomogeneous media in 3D. For isotropic inhomogeneous media we discuss the discrete equations on a staggered grid resulting in a unique way to discretize material parameters, and evaluate stability conditions and consistency for isotropic homogeneous unbounded media. For the sake of simplified visualization, numerical results are presented for various two-dimensional problems as they originate from nondestructive testing applications. In particular, EFIT wavefronts are related to group velocity curves for anisotropic media with transverse isotropy and cubic symmetry, the latter one being derived by a coordinate-free approach in the appendix.

1. Introduction

Particularly, seismological exploration and ultrasonic nondestructive testing require numerical modeling of radiation, propagation, and scattering of elastic waves. Unfortunately, analytical methods are only able to handle canonical problems, whereas real-life problems have to be tackled with numerical methods. These comprise semi-analytical techniques like the elastodynamic geometric theory of diffraction [1] and the boundary element method (BEM), which is based upon an elastodynamic version of Huygens' principle [2]; "purely" numerical techniques mainly operate directly on the fundamental equations of motion, among them finite difference time domain methods (FDTD) [3], velocity-stress FDTD (VS-FDTD) [4] and finite element methods (FE) [5]. Recently [6,7], we have proposed another scheme acronymed EFIT for elastodynamic finite integration technique, which has a successful counterpart in electromagnetics [8]. Several applications in nondestructive testing [9] proved its feasibility und utility, in particular for CAI (Computer Aided Inspection) [10], which combines modeling and imaging. For isotropic homogeneous media, the discrete EFIT equations are close to VS-FDTD, but for inhomogeneous media, the EFIT discretization proves superior. In the present paper we address the fundamental questions of stability, consistency, and convergence of the three-dimensional EFIT scheme, and discuss, for the sake of simplified visualization, some two-dimensional examples for isotropic inhomogeneous and anisotropic homogeneous media.

* Corresponding author.

SSDI 0165-2125(94)00040-9

2. Integral formulation of linear elastodynamic equations for anisotropic inhomogeneous media

Various textbooks [11–14] define the field variables of elastodynamics as function of time t and observation vector $\underline{\mathbf{R}}$:
- motion-related particle displacement velocity $\underline{\mathbf{v}}(\underline{\mathbf{R}}, t)$ and strain tensor $\underline{\underline{\mathbf{S}}}(\underline{\mathbf{R}}, t)$,
- force-related momentum density $\underline{\mathbf{p}}(\underline{\mathbf{R}}, t)$ and stress tensor $\underline{\underline{\mathbf{T}}}(\underline{\mathbf{R}}, t)$.

The equations of elastodynamics combine motion-related and force-related field variables via fundamental physical laws. It is most convenient to consider a finite volume V with surface S of the solid; via definition of its
- total momentum vector

$$\iiint_V \underline{\mathbf{p}}(\underline{\mathbf{R}}, t)\, \mathrm{d}V,$$

- total surface traction vector – $\underline{\mathbf{n}}$ denoting the outward normal unit vector on S –

$$\iint_S \underline{\mathbf{n}} \cdot \underline{\underline{\mathbf{T}}}(\underline{\mathbf{R}}, t)\, \mathrm{d}S,$$

- deformation volume second rank tensor

$$\iiint_V \underline{\underline{\mathbf{S}}}(\underline{\mathbf{R}}, t)\, \mathrm{d}V,$$

- and particle flux second rank tensor

$$\iint_S \underline{\mathbf{n}}\, \underline{\mathbf{v}}(\underline{\mathbf{R}}, t)\, \mathrm{d}S.$$

Newton's principle of linear momentum yields

$$\frac{\mathrm{d}}{\mathrm{d}t} \iiint_V \underline{\mathbf{p}}(\underline{\mathbf{R}}, t)\, \mathrm{d}V = \iint_S \underline{\mathbf{n}} \cdot \underline{\underline{\mathbf{T}}}(\underline{\mathbf{R}}, t)\, \mathrm{d}S. \tag{1}$$

According to the law of deformation, a particle flux results in a time variation of the deformation volume according to

$$\frac{\mathrm{d}}{\mathrm{d}t} \iiint_V \underline{\underline{\mathbf{S}}}(\underline{\mathbf{R}}, t)\, \mathrm{d}V = \iint_S \frac{1}{2} \left[\underline{\mathbf{n}}\, \underline{\mathbf{v}}(\underline{\mathbf{R}}, t) + \underline{\mathbf{v}}(\underline{\mathbf{R}}, t) \underline{\mathbf{n}}\right] \mathrm{d}S, \tag{2}$$

indicating that the antisymmetric particle flux only results in a rotation of the deformation volume, which does not contribute to its time variation, whence the symmetry of $\underline{\underline{\mathbf{S}}}(\underline{\mathbf{R}}, t)$.

Eqs. (1) and (2) represent the elastodynamic counterpart of Maxwell's equations of electromagnetics in integral form. If necessary, they can be augmented on the right hand side by an independent volume source term, respectively. This term is in Eq. (2).
- the integrated force density $\underline{\mathbf{f}}(\underline{\mathbf{R}}, t)$

$$\iiint_V \underline{\mathbf{f}}(\underline{\mathbf{R}}, t)\, \mathrm{d}V \tag{3}$$

and in Eq. (2)
- the integrated source of deformation rate $\underline{\underline{\mathbf{h}}}(\underline{\mathbf{R}}, t)$

$$\iiint_V \underline{\underline{\mathbf{h}}}(\underline{\mathbf{R}}, t)\, \mathrm{d}V . \tag{4}$$

As is well-known in electromagnetics, for "media" other than vacuum, *additional* constitutive equations are required to solve Maxwell's equations. The same holds for (1) and (2), where usually linearity comes in, i. e. $\underline{\mathbf{p}}$ and $\underline{\mathbf{v}}$ are related by a mass density tensor (at rest) $\underline{\underline{\boldsymbol{\varrho}}}_0(\underline{\mathbf{R}})$ according to

$$\underline{\mathbf{p}}(\underline{\mathbf{R}}, t) = \underline{\underline{\boldsymbol{\varrho}}}_0(\underline{\mathbf{R}}) \cdot \underline{\mathbf{v}}(\underline{\mathbf{R}}, t) , \tag{5}$$

and, similarly, $\underline{\underline{\mathbf{S}}}$ and $\underline{\underline{\mathbf{T}}}$ are related by the fourth rank compliance tensor $\underline{\underline{\underline{\underline{\mathbf{s}}}}}$ according to

$$\underline{\underline{\mathbf{S}}}(\underline{\mathbf{R}}, t) = \underline{\underline{\underline{\underline{\mathbf{s}}}}}(\underline{\mathbf{R}}) : \underline{\underline{\mathbf{T}}}(\underline{\mathbf{R}}, t) . \tag{6}$$

The double dot indicates double contraction [14]. Alternatively, (6) can be inverted

$$\underline{\underline{\mathbf{T}}}(\underline{\mathbf{R}}, t) = \underline{\underline{\underline{\underline{\mathbf{c}}}}}(\underline{\mathbf{R}}) : \underline{\underline{\mathbf{S}}}(\underline{\mathbf{R}}, t), \tag{7}$$

thus defining the fourth rank stiffness tensor of Hooke's law. To model elastic wave propagation and scattering, the material parameters $\underline{\underline{\boldsymbol{\varrho}}}_0(\underline{\mathbf{R}}), \underline{\underline{\underline{\underline{\mathbf{c}}}}}(\underline{\mathbf{R}}), \underline{\underline{\underline{\underline{\mathbf{s}}}}}(\underline{\mathbf{R}})$ have to be specified, in an inverse problem they have to be determined from field measurements.

Inserting the elastodynamic constitutive equations into the equations of motion (1) and(2) and ignoring higher order effects due to a time variation of V itself, we obtain

$$\iiint_V \underline{\underline{\boldsymbol{\varrho}}}_0(\underline{\mathbf{R}}) \cdot \dot{\underline{\mathbf{v}}}(\underline{\mathbf{R}}, t)\, \mathrm{d}V = \iint_S \underline{\mathbf{n}} \cdot \underline{\underline{\mathbf{T}}}(\underline{\mathbf{R}}, t)\, \mathrm{d}S, \tag{8}$$

$$\iiint_V \underline{\underline{\underline{\underline{\mathbf{s}}}}}(\underline{\mathbf{R}}) : \dot{\underline{\underline{\mathbf{T}}}}(\underline{\mathbf{R}}, t)\, \mathrm{d}V = \iint_S \frac{1}{2} \left[\underline{\mathbf{n}}\, \underline{\mathbf{v}}(\underline{\mathbf{R}}, t) + \underline{\mathbf{v}}(\underline{\mathbf{R}}, t) \underline{\mathbf{n}}\right] \mathrm{d}S, \tag{9}$$

the dot indicating first time derivative. These two equations – Cauchy's equation of motion and the deformation rate equation – represent the starting point for EFIT in anisotropic inhomogeneous media. In order not to complicate our discussion we first concentrate on isotropic inhomogeneous media.

For isotropic media, only a scalar mass density is required, and hence

$$\underline{\underline{\boldsymbol{\varrho}}}_0(\underline{\mathbf{R}}) = \varrho_0(\underline{\mathbf{R}}) \underline{\underline{\mathbf{I}}}, \tag{10}$$

with the unity tensor $\underline{\underline{\mathbf{I}}}$. Similarly, with the two independent Lamé's constants $\lambda(\underline{\mathbf{R}})$ and $\mu(\underline{\mathbf{R}})$, the stiffness tensor for isotropic media [1] is given by

$$\underline{\underline{\underline{\underline{\mathbf{c}}}}}(\underline{\mathbf{R}}) = \lambda(\underline{\mathbf{R}}) \underline{\underline{\mathbf{I}}}\, \underline{\underline{\mathbf{I}}} + \mu(\underline{\mathbf{R}}) \left(\underline{\underline{\mathbf{I}}}\, \underline{\underline{\mathbf{I}}}^{1324} + \underline{\underline{\mathbf{I}}}\, \underline{\underline{\mathbf{I}}}^{1342}\right) , \tag{11}$$

where we apply the upper indicial notation [2] of [14]. The compliance tensor for isotropic media has the same structure as (11), but [12]

[1] In Voigt's matrix notation we have $c_{11} = \lambda + 2\mu$ and $c_{44} = \mu$ with the isotropic symmetry condition $c_{12} = c_{11} - 2c_{44} = \lambda$.

[2] For instance, the transpose of a tensor $\underline{\underline{\mathbf{A}}}$ is written as $\underline{\underline{\mathbf{A}}}^{21}$; accordingly, $\underline{\underline{\mathbf{I}}}\, \underline{\underline{\mathbf{I}}}^{1342}$ is the identity operator with regard to double contraction, i.e. $\underline{\underline{\mathbf{A}}} : \underline{\underline{\mathbf{I}}}\, \underline{\underline{\mathbf{I}}}^{1342} = \underline{\underline{\mathbf{I}}}\, \underline{\underline{\mathbf{I}}}^{1342} : \underline{\underline{\mathbf{A}}} = \underline{\underline{\mathbf{A}}}$ and $\underline{\underline{\mathbf{A}}} : \underline{\underline{\mathbf{I}}}\, \underline{\underline{\mathbf{I}}}^{1324} = \underline{\underline{\mathbf{I}}}\, \underline{\underline{\mathbf{I}}}^{1324} : \underline{\underline{\mathbf{A}}} = \underline{\underline{\mathbf{A}}}^{21}$.

$$\underline{\underline{\underline{\underline{s}}}}(\underline{\mathbf{R}}) = \Lambda(\underline{\mathbf{R}})\underline{\underline{\underline{\underline{\mathbf{I}}}}}\,\underline{\underline{\mathbf{I}}} + M(\underline{\mathbf{R}})\left(\underline{\underline{\underline{\underline{\mathbf{I}}}}}^{1324} + \underline{\underline{\underline{\underline{\mathbf{I}}}}}^{1342}\right), \tag{12}$$

with

$$\Lambda(\underline{\mathbf{R}}) = -\frac{\lambda(\underline{\mathbf{R}})}{2\mu(\underline{\mathbf{R}})[3\lambda(\underline{\mathbf{R}}) + 2\mu(\underline{\mathbf{R}})]}, \tag{13}$$

$$M(\underline{\mathbf{R}}) = \frac{1}{4\mu(\underline{\mathbf{R}})}. \tag{14}$$

3. EFIT discretization for isotropic inhomogeneous media

The fundamental idea for EFIT is the Finite Integration Technique (FIT), which has been very successfully utilized to discretize Maxwell's equations [8]. To apply FIT to Eqs. (8) and (9) to yield EFIT as discussed in [6] for isotropic homogeneous media we evaluate the volume and surface integrals approximately for each cubic discretization volume $V = \Delta x^3$ assuming constant $\underline{\mathbf{v}}$ and $\underline{\underline{\mathbf{T}}}$ within V and on each of the six quadratic surfaces $S = \Delta x^2$ of V. Obviously, this requires staggered grids, which are centered around the cartesian components v_1, v_2, v_3 of $\underline{\mathbf{v}}$, and around the main and off-diagonal elements $T_{11}, T_{22}, T_{33}, T_{12}, T_{13}, T_{23}$ of $\underline{\underline{\mathbf{T}}}$. Careful investigation of the respective components necessary for either (8) or (9) results – in case of isotropic homogeneous media – in the location of components as displayed in Fig. 1, which, interesting enough, is appropriate for both Cauchy- and deformation rate equations, and, concerning the latter, for both main and off-diagonal elements of $\underline{\underline{\mathbf{T}}}$. From the nine integration volumes we extract the EFIT-$\underline{\mathbf{v}}$-grid (compare Fig. 1), which is staggered with regard to the "dual" EFIT-$\underline{\underline{\mathbf{T}}}$-grid, the latter one being similarly organized than the $\underline{\mathbf{v}}$-grid by the $T_{ij,i\neq j}$-components; it is centered around the T_{ii}-components.

In the case of inhomogeneous media a discretization of the material parameter distribution has to be introduced, which cannot be done arbitrarily, because continuity of $\underline{\mathbf{n}}\cdot\underline{\underline{\mathbf{T}}}$ and $\underline{\mathbf{v}}$ has to be ensured on its grid surfaces, and these transition conditions should involve only *those* components of the EFIT-discretization grid which *are* continuous on the material discretization grid. For instance, if the $\dot{v}_1$-integration cube of Fig. 1 would coincide with a cube of the material parameter grid, continuity of T_{11} would be required on the left boundary; but on this boundary, EFIT requires $\underline{\underline{\mathbf{T}}}$-components T_{22} and T_{33} also, which are not supposed to be continuous. Accordingly, this discretization of material parameters is not appropriate for EFIT and does not lead to stable results. As a matter of fact, it turns out, that there is only *one* appropriate discretization for material parameters, which should coincide with the "dual" EFIT-$\underline{\underline{\mathbf{T}}}$-grid; this is the essential difference of EFIT compared to [4]. Then, for isotropic inhomogeneous media the following discrete EFIT equations are obtained, where M_i, $i = 1,2,3$ denote the node number distance in x_i-direction of the node adjacent to node n:

$$\dot{v}_1^{(n)}(t) = \frac{1}{\Delta x}\frac{2}{\varrho_0^{(n)} + \varrho_0^{(n+M_1)}} \times \left[T_{11}^{(n+M_1)}(t) - T_{11}^{(n)}(t) + T_{12}^{(n)}(t) - T_{12}^{(n-M_2)}(t) + T_{13}^{(n)}(t) - T_{13}^{(n-M_3)}(t)\right], \tag{15}$$

$$\dot{v}_2^{(n)}(t) = \frac{1}{\Delta x}\frac{2}{\varrho_0^{(n)} + \varrho_0^{(n+M_2)}} \times \left[T_{12}^{(n)}(t) - T_{12}^{(n-M_1)}(t) + T_{22}^{(n+M_2)}(t) - T_{22}^{(n)}(t) + T_{23}^{(n)}(t) - T_{23}^{(n-M_3)}(t)\right], \tag{16}$$

$$\dot{v}_3^{(n)}(t) = \frac{1}{\Delta x}\frac{2}{\varrho_0^{(n)} + \varrho_0^{(n+M_3)}} \times \left[T_{13}^{(n)}(t) - T_{13}^{(n-M_1)}(t) + T_{23}^{(n)}(t) - T_{23}^{(n-M_2)}(t) + T_{33}^{(n+M_3)}(t) - T_{33}^{(n)}(t)\right], \tag{17}$$

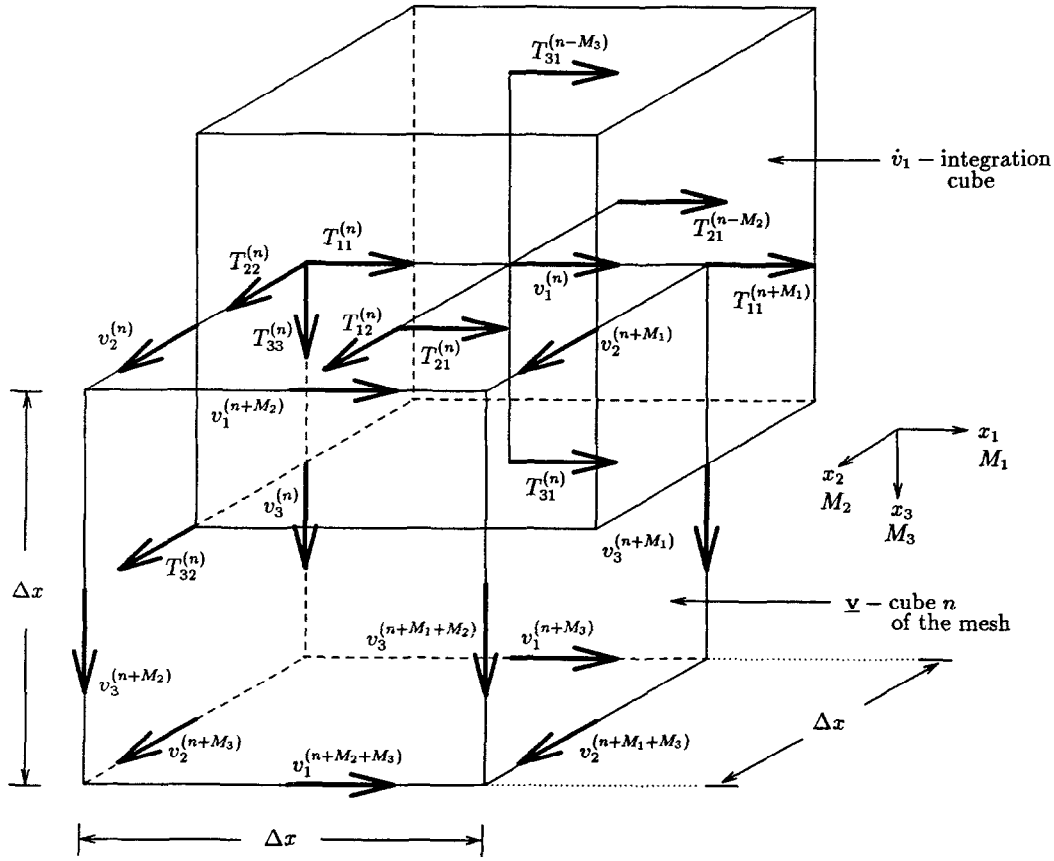

Fig. 1. Staggered grid for EFIT for a particular node number n; T-cube s not shown.

$$\dot{T}_{11}^{(n)}(t) = \frac{1}{\Delta x}\left\{\left(\lambda^{(n)} + 2\mu^{(n)}\right)\left[v_1^{(n)}(t) - v_1^{(n-M_1)}(t)\right] + \lambda^{(n)}\left[v_2^{(n)}(t) - v_2^{(n-M_2)}(t) + v_3^{(n)}(t) - v_3^{(n-M_3)}(t)\right]\right\}, \tag{18}$$

$$\dot{T}_{22}^{(n)}(t) = \frac{1}{\Delta x}\left\{\left(\lambda^{(n)} + 2\mu^{(n)}\right)\left[v_2^{(n)}(t) - v_2^{(n-M_2)}(t)\right] + \lambda^{(n)}\left[v_1^{(n)}(t) - v_1^{(n-M_1)}(t) + v_3^{(n)}(t) - v_3^{(n-M_3)}(t)\right]\right\}, \tag{19}$$

$$\dot{T}_{33}^{(n)}(t) = \frac{1}{\Delta x}\left\{\left(\lambda^{(n)} + 2\mu^{(n)}\right)\left[v_3^{(n)}(t) - v_3^{(n-M_3)}(t)\right] + \lambda^{(n)}\left[v_1^{(n)}(t) - v_1^{(n-M_1)}(t) + v_2^{(n)}(t) - v_2^{(n-M_2)}(t)\right]\right\}, \tag{20}$$

$$\dot{T}_{12}^{(n)}(t) = \frac{1}{\Delta x}\frac{4}{\dfrac{1}{\mu^{(n)}} + \dfrac{1}{\mu^{(n+M_1)}} + \dfrac{1}{\mu^{(n+M_2)}} + \dfrac{1}{\mu^{(n+M_1+M_2)}}} \times \left[v_1^{(n+M_2)}(t) - v_1^{(n)}(t) + v_2^{(n+M_1)}(t) - v_2^{(n)}(t)\right], \tag{21}$$

$$\dot{T}_{13}^{(n)}(t) = \frac{1}{\Delta x} \frac{4}{\frac{1}{\mu^{(n)}} + \frac{1}{\mu^{(n+M_1)}} + \frac{1}{\mu^{(n+M_3)}} + \frac{1}{\mu^{(n+M_1+M_3)}}} \times \left[v_1^{(n+M_3)}(t) - v_1^{(n)}(t) + v_3^{(n+M_1)}(t) - v_3^{(n)}(t) \right], \tag{22}$$

$$\dot{T}_{23}^{(n)}(t) = \frac{1}{\Delta x} \frac{4}{\frac{1}{\mu^{(n)}} + \frac{1}{\mu^{(n+M_2)}} + \frac{1}{\mu^{(n+M_3)}} + \frac{1}{\mu^{(n+M_2+M_3)}}} \times \left[v_2^{(n+M_3)}(t) - v_2^{(n)}(t) + v_3^{(n+M_2)}(t) - v_3^{(n)}(t) \right]. \tag{23}$$

Notice, for the $\dot{T}_{11/22/33}$-equations only material parameters of cube n of the EFIT grid are involved, and, therefore, the $\underline{\underline{\mathbf{s}}}$:-operation can be inverted for each cube to yield the stiffness formulation as inhomogeneous media.

Of course, if the medium is inhomogeneously anisotropic, the same ideas as above apply.

The time derivative in (15)-(23) is approximated by central differences according to

$$\boldsymbol{v}_i^{(z)} = \boldsymbol{v}_i^{(z-1)} + \dot{\boldsymbol{v}}_i^{(z-1/2)} \Delta t, \tag{24}$$

$$\boldsymbol{T}_{ij}^{(z+1/2)} = \boldsymbol{T}_{ij}^{(z-1/2)} + \dot{\boldsymbol{T}}_{ij}^{(z)} \Delta t, \quad i,j = 1,2,3, \tag{25}$$

yielding a leap-frog integration scheme. In (24) and (25), $\boldsymbol{v}_i^{(z)}$ denotes the vector composed of particle velocity components v_i for all nodes n for a certain time $t = z\Delta t$ with integer z; $\boldsymbol{T}_{ij}^{(z)}$ is similarly defined.

A number of 2D numerical results for nondestructive testing – transducer radiation into solids and scattering by defects in homogeneous media – are available in [9,10,15], and [9,10] also contain the "extension" of EFIT to purely acoustic waves, acronymed AFIT for Acoustic Finite Integration Technique [16]. In two dimensions EFIT results have additionally been validated against analytical solutions [7] and a particular Finite Element code [17] described in [5].

4. Stability of EFIT for isotropic homogeneous unbounded media

4.1. Stability of EFIT in 3D

Let us consider a slight generalization of our cubic EFIT grid in terms of unequal lateral dimensions $\Delta x_1, \Delta x_2, \Delta x_3$ of the grid volume V, and let us further define grid nodes through the following numbering

$$\text{1-direction}: i_1 = 1,2,\ldots,I_1,$$

$$\text{2-direction}: i_2 = 1,2,\ldots,I_2,$$

$$\text{3-direction}: i_3 = 1,2,\ldots,I_3,$$

yielding node $n = n(i_1,i_2,i_3)$ through

$$n(i_1,i_2,i_3) = 1 + (i_1 - 1) + (i_2 - 1)I_1 + (i_3 - 1)I_1I_2, \tag{26}$$

if we move through the grid in $(1 \longrightarrow 2 \longrightarrow 3)$-direction. Stability of the numerical marching-in-time scheme is investigated discussing the behavior of Eqs. (15)-(23) – as specified for homogeneous media – simultaneously for all nodes when time is incremented by Δt from $z\Delta t$ to $(z+1)\Delta t$. To do this we make a time harmonic

plane wave ansatz for all field components as proposed by J. von Neumann [18], for instance in terms of the particle velocity for the coordinates of node n and time $z\Delta t$

$$v_i^{(n,z)} = v_{i0}^{(i_1,i_2,i_3,z)}(\omega_0)\mathrm{e}^{j(k_1 i_1 \Delta x_1 + k_2 i_2 \Delta x_2 + k_3 i_3 \Delta x_3)}\mathrm{e}^{-j\omega_0 z\Delta t}, \tag{27}$$

where $k_i, i = 1,2,3$ denote the cartesian components of the wave number vector. Inserting this ansatz into (15)-(23) with reference to Fig. 1 regarding the relative dislocation of components, and observing (24) and (25) we obtain straightforwardly the following matrix equation

$$\underline{\boldsymbol{u}}^{(z+1/2)} = \underline{\boldsymbol{u}}^{(z-1/2)} + \underline{\underline{\boldsymbol{A}}} \cdot \underline{\boldsymbol{u}}^{(z)}, \tag{28}$$

with

$$\underline{\underline{\boldsymbol{A}}} = \begin{pmatrix} 0 & 0 & 0 & 2j\chi_1 & 0 & 0 & 0 & 2j\chi_3 & 2j\chi_2 \\ 0 & 0 & 0 & 0 & 2j\chi_2 & 0 & 2j\chi_3 & 0 & 2j\chi_1 \\ 0 & 0 & 0 & 0 & 0 & 2j\chi_3 & 2j\chi_2 & 2j\chi_1 & 0 \\ 2j\chi_1 & 2jb\chi_2 & 2jb\chi_3 & 0 & 0 & 0 & 0 & 0 & 0 \\ 2jb\chi_1 & 2j\chi_2 & 2jb\chi_3 & 0 & 0 & 0 & 0 & 0 & 0 \\ 2jb\chi_1 & 2jb\chi_2 & 2j\chi_3 & 0 & 0 & 0 & 0 & 0 & 0 \\ 0 & 2ja\chi_3 & 2ja\chi_2 & 0 & 0 & 0 & 0 & 0 & 0 \\ 2ja\chi_3 & 0 & 2ja\chi_1 & 0 & 0 & 0 & 0 & 0 & 0 \\ 2ja\chi_2 & 2ja\chi_1 & 0 & 0 & 0 & 0 & 0 & 0 & 0 \end{pmatrix}. \tag{29}$$

Here, stimulated by the stability investigations of Taflove and Brodwin [19] for the electromagnetic case, the 9-component "field"-vector $\underline{\boldsymbol{u}}^{(z)}$ is defined by

$$\underline{\boldsymbol{u}}^{(z)} = \begin{pmatrix} v_1^{(z)} \\ v_2^{(z)} \\ v_3^{(z)} \\ \eta_P T_{11}^{(z)} \\ \eta_P T_{22}^{(z)} \\ \eta_P T_{33}^{(z)} \\ \eta_P T_{23}^{(z)} \\ \eta_P T_{13}^{(z)} \\ \eta_P T_{12}^{(z)} \end{pmatrix}, \tag{30}$$

with the elastic pressure wave impedance

$$\eta_P = 1/\sqrt{\varrho_0(\lambda + 2\mu)}. \tag{31}$$

The quantities a and b are related to the pressure and shear wave speeds

$$c_P = \sqrt{(\lambda + 2\mu)/\varrho_0}, \tag{32}$$

$$c_S = \sqrt{\mu/\varrho_0}, \tag{33}$$

through

$$a = c_S^2/c_P^2, \tag{34}$$

$$b = 1 - 2a. \tag{35}$$

The grid and the wave number components k_i of the plane wave are hidden in

$$\chi_i = c_P \frac{\Delta t}{\Delta x_i} \sin\left(\frac{k_i \Delta x_i}{2}\right), \quad i = 1,2,3. \tag{36}$$

Eliminating the half-time step $\underline{\mathcal{U}}^{(z-1/2)}$ in (28) through definition of

$$\underline{\mathcal{V}}^{(z)} = \underline{\mathcal{U}}^{(z-1/2)}, \tag{37}$$

we obtain the final matrix equation

$$\underline{\mathcal{W}}^{(z+1/2)} = \underbrace{\begin{pmatrix} \underline{\underline{\mathcal{A}}} & \underline{\underline{\mathcal{I}}} \\ \underline{\underline{\mathcal{I}}} & \underline{\underline{\mathcal{O}}} \end{pmatrix}}_{=\underline{\underline{\mathcal{G}}}} \cdot \underline{\mathcal{W}}^{(z)}, \tag{38}$$

if $\underline{\mathcal{W}}^{(z)}$ is given by

$$\underline{\mathcal{W}}^{(z)} = \begin{pmatrix} \underline{\mathcal{U}}^{(z)} \\ \underline{\mathcal{V}}^{(z)} \end{pmatrix}; \tag{39}$$

$\underline{\underline{\mathcal{I}}}$ denotes the 9×9-identity and $\underline{\underline{\mathcal{O}}}$ the corresponding null matrix. The matrix $\underline{\underline{\mathcal{G}}}$ is called the amplification matrix, and according to J. von Neumann [18], a numerical scheme is stable provided the absolute value of the eigenvalues ν_m of $\underline{\underline{\mathcal{G}}}$ is not greater than one, i. e.

$$|\nu_m| \leq 1 \quad \text{for } m = 1, \ldots, 18. \tag{40}$$

The explicit expression for the characteristic polynomial $P_{3D}(\nu)$ of $\underline{\underline{\mathcal{G}}}$ in three dimensions is given by

$$\begin{aligned} P_{3D}(\nu) = \alpha^3 \{ & \alpha^6 + 4\alpha^4 \nu^2 (1+2a) \left(\chi_1^2 + \chi_2^2 + \chi_3^2\right) \\ & + 16\alpha^2 \nu^4 a (2+a) \left(\chi_1^2 + \chi_2^2 + \chi_3^2\right)^2 + 64\nu^6 a^2 \left(\chi_1^2 + \chi_2^2 + \chi_3^2\right)^3 \}, \end{aligned} \tag{41}$$

with $\alpha = \nu^2 - 1$. As eigenvalues, $\nu_{1/3/5} = 1$ and $\nu_{2/4/6} = -1$ are immediately recognized; substituting $\mu = \alpha^2$ in the bracketed 6th order polynominal, it factorizes in the form

$$\left[\mu + 4\nu^2 \left(\chi_1^2 + \chi_2^2 + \chi_3^2\right)\right] \left[\mu + 4\nu^2 a \left(\chi_1^2 + \chi_2^2 + \chi_3^2\right)\right]^2. \tag{42}$$

Therefore the zeros in μ of the 6th order polynominal are

$$\mu_1 = -4\nu^2 \left(\chi_1^2 + \chi_2^2 + \chi_3^2\right), \tag{43}$$

$$\mu_{2/3} = -4\nu^2 a \left(\chi_1^2 + \chi_2^2 + \chi_3^2\right). \tag{44}$$

For the μ_1-equation the eigenvalues

$$\nu_{7/8/9/10} = \pm j \sqrt{\chi_1^2 + \chi_2^2 + \chi_3^2} \pm \sqrt{1 - \left(\chi_1^2 + \chi_2^2 + \chi_3^2\right)} \tag{45}$$

are obtained, whereas the second $\mu_{2/3}$-equations yield

$$\nu_{11/12/13/14} = \pm j \sqrt{a \left(\chi_1^2 + \chi_2^2 + \chi_3^2\right)} \pm \sqrt{1 - a \left(\chi_1^2 + \chi_2^2 + \chi_3^2\right)} = \nu_{15/16/17/18}. \tag{46}$$

To ensure $|\nu_{7/8/9/10}| \leq 1$, we have to require

$$\chi_1^2 + \chi_2^2 + \chi_3^2 \leq 1, \tag{47}$$

resulting in

$$\Delta t \leq \frac{1}{c_P} \frac{1}{\sqrt{1/\Delta x_1^2 + 1/\Delta x_2^2 + 1/\Delta x_3^2}} . \tag{48}$$

Because $c_S \leq c_P$ we always have $a \leq 1$, and therefore condition (48) also ensures $|\nu_{11-18}| \leq 1$. Obviously, (48) complies with Taflove's and Brodwin's result for the electromagnetic case [19], and it extends the well-known Courant-Friedrichs-Lewy stability criterion of one-dimensional FDTD methods [18,20,21] to higher dimensions.

Stability of EFIT with regard to time is related to the highest wave speed, whereas spatial discretization is related to the lowest wave speed. We applied the stability criterion (48) also to bounded media and never encountered any difficulty.

4.2. Stability of EFIT in 2D

In two dimensions, if the plane strain hypothesis is hold [14] – parallel to the x_1x_3 plane – the same procedure as above yields with

$$\underline{\underline{A}} = \begin{pmatrix} 0 & 0 & 2j\chi_1 & 0 & 2j\chi_3 \\ 0 & 0 & 0 & 2j\chi_3 & 2j\chi_1 \\ 2j\chi_1 & 2jb\chi_3 & 0 & 0 & 0 \\ 2jb\chi_1 & 2j\chi_3 & 0 & 0 & 0 \\ 2ja\chi_3 & 2ja\chi_1 & 0 & 0 & 0 \end{pmatrix} \tag{49}$$

the characteristic polynominal in two dimensions

$$P_{2D}(\nu) = \alpha \left[\alpha^4 + 4\alpha^2\nu^2(1+a)(\chi_1^2+\chi_3^2) + 16a\nu^4(\chi_1^2+\chi_3^2)^2\right], \tag{50}$$

with $\alpha = \nu^2 - 1$. As eigenvalues, $\nu_{1/2} = \pm 1$ are immediately recognized; substituting $\mu = \alpha^2$ in the bracketed factor we find

$$\mu_{1/2} = -2\nu^2(1+a)(\chi_1^2+\chi_3^2) \pm 2\nu^2(1-a)(\chi_1^2+\chi_3^2) . \tag{51}$$

For the lower sign in (51) the eigenvalues

$$\nu_{3/4/5/6} = \pm j\sqrt{\chi_1^2+\chi_3^2} \pm \sqrt{1-(\chi_1^2+\chi_3^2)} \tag{52}$$

are obtained, whereas the upper sign yields

$$\nu_{7/8/9/10} = \pm j\sqrt{a(\chi_1^2+\chi_3^2)} \pm \sqrt{1-a(\chi_1^2+\chi_3^2)} . \tag{53}$$

To ensure $|\nu_{3/4/5/6}| \leq 1$, we have to require

$$\chi_1^2 + \chi_3^2 \leq 1, \tag{54}$$

resulting in

$$\Delta t \leq \frac{1}{c_P} \frac{1}{\sqrt{1/\Delta x_1^2 + 1/\Delta x_3^2}} . \tag{55}$$

This is the stability condition of the 2D EFIT scheme related to the highest wave speed. We applied this criterion (55) to bounded homogeneous, inhomogeneous and anisotropic media. For an inhomogeneous medium c_P must

be replaced by c_{Pmax} which is the maximum phase velocity expected within the spatial domain. Further, in the anisotropic case c_{P} must be replaced by $c_{g\mathrm{Pmax}}$ which is the maximum group velocity.

5. Dispersion relations, consistency, and convergence of EFIT for isotropic homogeneous unbounded media

5.1. Dispersion relations of EFIT in 3D

If a numerical scheme is consistent in the sense that its discrete dispersion relation has the pertinent "continuous" dispersion relation as a limit, then the Lax equivalence theorem [18,21] ensures convergence provided the stability condition is satisfied.

Consistency of the 3D EFIT scheme is explicitly shown in the following for isotropic homogeneous media.

Suppressing the term $\mathrm{e}^{-j\omega_0 z\Delta t}$ in (28) by defining "phasors"

$$\underline{\mathcal{U}} = \underline{\mathcal{U}}^{(z)}\mathrm{e}^{j\omega_0 z\Delta t}, \tag{56}$$

we obtain instead of (28)

$$\underline{\underline{\mathcal{D}}}\cdot\underline{\mathcal{U}} = 0, \tag{57}$$

with

$$\underline{\underline{\mathcal{D}}} = 2j\chi_t\underline{\underline{\mathcal{I}}} + \underline{\underline{\mathcal{A}}} \tag{58}$$

$$= \begin{pmatrix} 2j\chi_t & 0 & 0 & 2j\chi_1 & 0 & 0 & 0 & 2j\chi_3 & 2j\chi_2 \\ 0 & 2j\chi_t & 0 & 0 & 2j\chi_2 & 0 & 2j\chi_3 & 0 & 2j\chi_1 \\ 0 & 0 & 2j\chi_t & 0 & 0 & 2j\chi_3 & 2j\chi_2 & 2j\chi_1 & 0 \\ 2j\chi_1 & 2jb\chi_2 & 2jb\chi_3 & 2j\chi_t & 0 & 0 & 0 & 0 & 0 \\ 2jb\chi_1 & 2j\chi_2 & 2jb\chi_3 & 0 & 2j\chi_t & 0 & 0 & 0 & 0 \\ 2jb\chi_1 & 2jb\chi_2 & 2j\chi_3 & 0 & 0 & 2j\chi_t & 0 & 0 & 0 \\ 0 & 2ja\chi_3 & 2ja\chi_2 & 0 & 0 & 0 & 2j\chi_t & 0 & 0 \\ 2ja\chi_3 & 0 & 2ja\chi_1 & 0 & 0 & 0 & 0 & 2j\chi_t & 0 \\ 2ja\chi_2 & 2ja\chi_1 & 0 & 0 & 0 & 0 & 0 & 0 & 2j\chi_t \end{pmatrix}, \tag{59}$$

and

$$\chi_t = \sin\left(\frac{\omega_0\Delta t}{2}\right). \tag{60}$$

Eq. (57) is a homogeneous "wave equation" for the discrete elastodynamic field in frequency-wave-number space. Hence, putting the determinant of $\underline{\underline{\mathcal{D}}}$ equal to zero yields the discrete dispersion relation.

Obviously $\det\underline{\underline{\mathcal{D}}} = 0$ yields a polynominal in χ_t, i. e.

$$\begin{aligned}\det\underline{\underline{\mathcal{D}}} = -512j\chi_t^3\{&-\chi_t^6 + \chi_t^4(1+2a)\left(\chi_1^2+\chi_2^2+\chi_3^2\right) \\ &-\chi_t^2 a(2+a)\left(\chi_1^2+\chi_2^2+\chi_3^2\right)^2 + a^2\left(\chi_1^2+\chi_2^2+\chi_3^2\right)^3\}.\end{aligned} \tag{61}$$

Factorization of the bracketed 6th order polynominal in χ_t yields

$$\left(-\chi_t^2+\chi_1^2+\chi_2^2+\chi_3^2\right)\left[-\chi_t^2 + a\left(\chi_1^2+\chi_2^2+\chi_3^2\right)\right]^2. \tag{62}$$

Therefore the nontrivial solutions are readily obtained as

$$\chi_{t1}^2 = \chi_1^2 + \chi_2^2 + \chi_3^2, \tag{63}$$

$$\chi_{t2/3}^2 = a(\chi_1^2 + \chi_2^2 + \chi_3^2)\,. \tag{64}$$

Explicit writing reveals the discrete dispersion relations of the pressure and shear wave with the phase velocities c_P and c_S

$$\frac{1}{c_P^2 \Delta t^2} \sin^2\left(\frac{\omega_0 \Delta t}{2}\right) = \frac{1}{\Delta x_1^2} \sin^2\left(\frac{k_1 \Delta x_1}{2}\right) + \frac{1}{\Delta x_2^2} \sin^2\left(\frac{k_2 \Delta x_2}{2}\right) + \frac{1}{\Delta x_3^2} \sin^2\left(\frac{k_3 \Delta x_3}{2}\right), \tag{65}$$

$$\frac{1}{c_S^2 \Delta t^2} \sin^2\left(\frac{\omega_0 \Delta t}{2}\right) = \frac{1}{\Delta x_1^2} \sin^2\left(\frac{k_1 \Delta x_1}{2}\right) + \frac{1}{\Delta x_2^2} \sin^2\left(\frac{k_2 \Delta x_2}{2}\right) + \frac{1}{\Delta x_3^2} \sin^2\left(\frac{k_3 \Delta x_3}{2}\right)\,. \tag{66}$$

The discrete dispersion relations (65) and (66) can be utilized to quatitatively determine the numerical phase velocities, numerical wave numbers, and numerical group velocities of the 3D EFIT scheme as a function of Δt, Δx_1, Δx_2, Δx_3 and propagation direction.

In the limit $\Delta t \longrightarrow 0, \Delta x_1 \longrightarrow 0, \Delta x_2 \longrightarrow 0, \Delta x_3 \longrightarrow 0$ the discrete dispersion relations (65) and (66) reach the "continuous" dispersion relations for (plane) pressure and shear waves

$$\omega_0^2 / {c_{P,S}}^2 = k_1^2 + k_2^2 + k_3^2, \tag{67}$$

as they are, for instance, obtained by a plane wave ansatz for the wave equations of the elastodynamic Helmholtz potentials [12].

Consequently, we have proven consistency of the 3D EFIT scheme.

Furthermore, this suggests that numerical dispersion effects can be reduced to any degree that is desired if we only use a fine-enough grid spacing.

5.2. *Dispersion relations of EFIT in 2D*

Investigating now the 2D case as in the previous section, $\underline{\underline{\mathcal{D}}}$ reduces to

$$\underline{\underline{\mathcal{D}}} = \begin{pmatrix} 2j\chi_t & 0 & 2j\chi_1 & 0 & 2j\chi_3 \\ 0 & 2j\chi_t & 0 & 2j\chi_3 & 2j\chi_1 \\ 2j\chi_1 & 2jb\chi_3 & 2j\chi_t & 0 & 0 \\ 2jb\chi_1 & 2j\chi_3 & 0 & 2j\chi_t & 0 \\ 2ja\chi_3 & 2ja\chi_1 & 0 & 0 & 2j\chi_t \end{pmatrix}, \tag{68}$$

and $\det\underline{\underline{\mathcal{D}}} = 0$ yields

$$\det\underline{\underline{\mathcal{D}}} = 32j\chi_t \left[\chi_t^4 - \chi_t^2(1+a)(\chi_1^2 + \chi_3^2) + a(\chi_1^2 + \chi_3^2)^2\right] = 0\,, \tag{69}$$

with the nontrivial solutions

$$\chi_t^2 = \chi_1^2 + \chi_3^2, \tag{70}$$

$$\chi_t^2 = a(\chi_1^2 + \chi_3^2) \tag{71}$$

and resulting in the discrete dispersion relations of the 2D EFIT scheme

$$\frac{1}{c_{P,S}^2 \Delta t^2} \sin^2\left(\frac{\omega_0 \Delta t}{2}\right) = \frac{1}{\Delta x_1^2} \sin^2\left(\frac{k_1 \Delta x_1}{2}\right) + \frac{1}{\Delta x_3^2} \sin^2\left(\frac{k_3 \Delta x_3}{2}\right)\,. \tag{72}$$

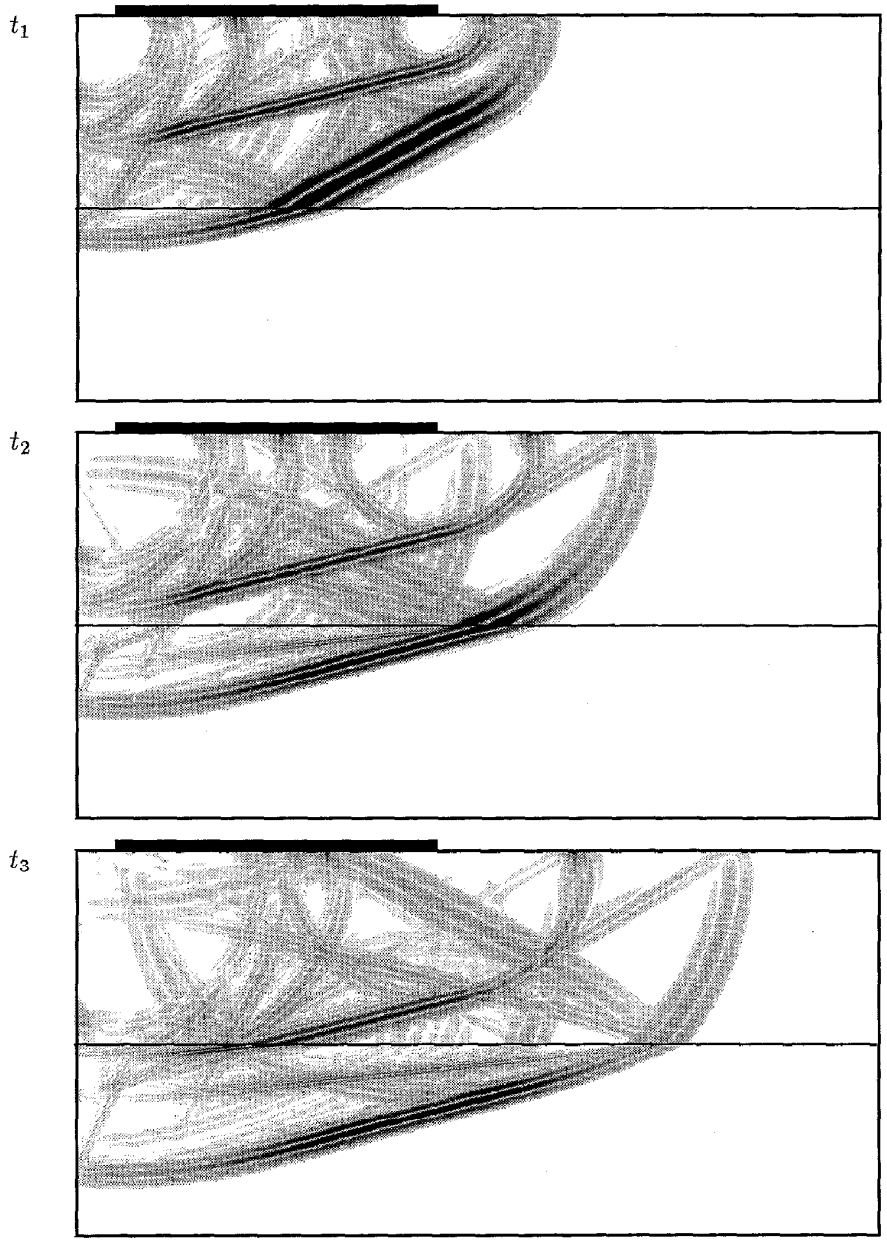

Fig. 2. Reflection, diffraction and mode conversion of finite aperture radiation by a plane boundary separating two homogeneous isotropic media (above boundary: Aluminium (polycrystal) with $c_P = 6420$ m/s, $c_S = 3040$ m/s and $\varrho_0 = 2700$ kg/m^3; below boundary: Zirconium with $c_P = 4650$ m/s, $c_S = 2250$ m/s and $\varrho_0 = 6490$ kg/m^3)

6. Numerical results

For the sake of simplicity we discuss only two-dimensional examples in the following.

Fig. 2 models transducer radiation into a two-layer isotropic specimen with stress-free boundaries in terms of time domain wavefront snap-shots. The excitation is in terms of a prescription of the normal component of the

stress tensor within a finite aperture; the spatial distribution is homogeneous, and the time variation is a finite bandwidth high-frequency pulse with linear retardation along the aperture resulting in a "steered beam" of both pressure and shear waves. These are then reflected, mode converted and diffracted at the interface between the two layers.

Fig. 3 models the elastic radiation field of a line force in a transversely isotropic homogeneous solid; obviously, the EFIT wavefronts comply well with the group velocity diagram as it is computed by the method described in the appendix.

Fig. 4 models transducer radiation into a transversely isotropic medium, and Fig. 5 gives an example of crack scattering in such a host material. It is interesting to observe the quasi-shear vertical wavefront cusps as they originate from the tips. Fig. 6 gives another example of line force radiation into a transversely isotropic medium, which has been deliberately chosen, because the pertinent wavefronts were recently derived by an analytic method [22]; of course, there is coincidence, but it should be emphasized, that EFIT gives also the amplitude distribution on the wavefronts. Fig. 6 also displays the group velocity diagrams.

Fig. 7 now turns to the case of an anisotropic solid with cubic symmetry; the line force EFIT wavefronts are once again compared to the group velocity diagrams.

Appendix A. Phase and group velocity for anisotropic media with transverse isotropy and cubic symmetry: a coordinate-free approach

The EFIT wavefronts of Figs. 3, 6 and 7 for anisotropic homogeneous media are explicitly related to the directional variation of the pertinent group velocity of plane waves [23]. To demonstrate this explicitly, we apply the formalism in [24], and describe a coordinate-free derivation of phase and group velocity for anisotropic media with transverse isotropy and with cubic symmetry.

From the differential formulation of Cauchy's equation of motion (6) and the deformation rate equation (7) a Navier-type differential equation

$$\nabla \cdot \underset{\equiv}{\mathbf{c}} \cdot \nabla \underline{\mathbf{u}}(\underline{\mathbf{R}}, t) - \varrho_0 \frac{\partial^2}{\partial t^2} \underline{\mathbf{u}}(\underline{\mathbf{R}}, t) = 0 \tag{A.1}$$

is derived for the displacement vector, which defines $\underline{\mathbf{v}}(\underline{\mathbf{R}}, t)$ through its first time derivative, i.e. $\underline{\mathbf{v}}(\underline{\mathbf{R}}, t) = \dot{\underline{\mathbf{u}}}(\underline{\mathbf{R}}, t)$; ∇ denotes the del-operator. Applying Fourier transforms with respect to time and space to (A.1) according to

$$\underline{\mathbf{u}}(\underline{\mathbf{K}}, \omega) = \int_{-\infty}^{+\infty} \int_{-\infty}^{+\infty} \int_{-\infty}^{+\infty} \int_{-\infty}^{+\infty} \underline{\mathbf{u}}(\underline{\mathbf{R}}, t) \mathrm{e}^{-j(\underline{\mathbf{K}} \cdot \underline{\mathbf{R}} - \omega t)} \, \mathrm{d}^3 \underline{\mathbf{R}} \, \mathrm{d}t, \tag{A.2}$$

with Fourier variables $\underline{\mathbf{K}}$ and ω we obtain

$$\underline{\underline{\mathbf{W}}}(\underline{\mathbf{K}}, \omega) \cdot \underline{\mathbf{u}}(\underline{\mathbf{K}}, \omega) = 0, \tag{A.3}$$

with the wave tensor

$$\underline{\underline{\mathbf{W}}}(\underline{\mathbf{K}}, \omega) = \underline{\mathbf{K}} \cdot \underset{\equiv}{\mathbf{c}} \cdot \underline{\mathbf{K}} - \varrho_0 \omega^2 \underline{\underline{\mathbf{I}}}. \tag{A.4}$$

For transversely isotropic media (crystals with hexagonal symmetry) the stiffness tensor reads [25,26]

$$\begin{aligned} \underset{\equiv}{\mathbf{c}}^{\mathrm{TI}} = {} & (c_{22} - 2c_{44}) \, \underline{\underline{\mathbf{I}}} \, \underline{\underline{\mathbf{I}}} + c_{44} \left(\underline{\underline{\mathbf{I}}} \, \underline{\underline{\mathbf{I}}}^{1324} + \underline{\underline{\mathbf{I}}} \, \underline{\underline{\mathbf{I}}}^{1342} \right) + \left[c_{11} + c_{22} - 2 \left(c_{12} + 2c_{55} \right) \right] \underline{\mathbf{a}} \, \underline{\mathbf{a}} \, \underline{\mathbf{a}} \, \underline{\mathbf{a}} \\ & + (c_{12} - c_{22} + 2c_{44}) \left(\underline{\underline{\mathbf{I}}} \, \underline{\mathbf{a}} \, \underline{\mathbf{a}} + \underline{\mathbf{a}} \, \underline{\mathbf{a}} \, \underline{\underline{\mathbf{I}}} \right) + (c_{55} - c_{44}) \left(\underline{\underline{\mathbf{I}}} \, \underline{\mathbf{a}} \, \underline{\mathbf{a}}^{1324} + \underline{\underline{\mathbf{I}}} \, \underline{\mathbf{a}} \, \underline{\mathbf{a}}^{1342} + \underline{\mathbf{a}} \, \underline{\mathbf{a}} \, \underline{\underline{\mathbf{I}}}^{1324} + \underline{\mathbf{a}} \, \underline{\mathbf{a}} \, \underline{\underline{\mathbf{I}}}^{1342} \right), \end{aligned} \tag{A.5}$$

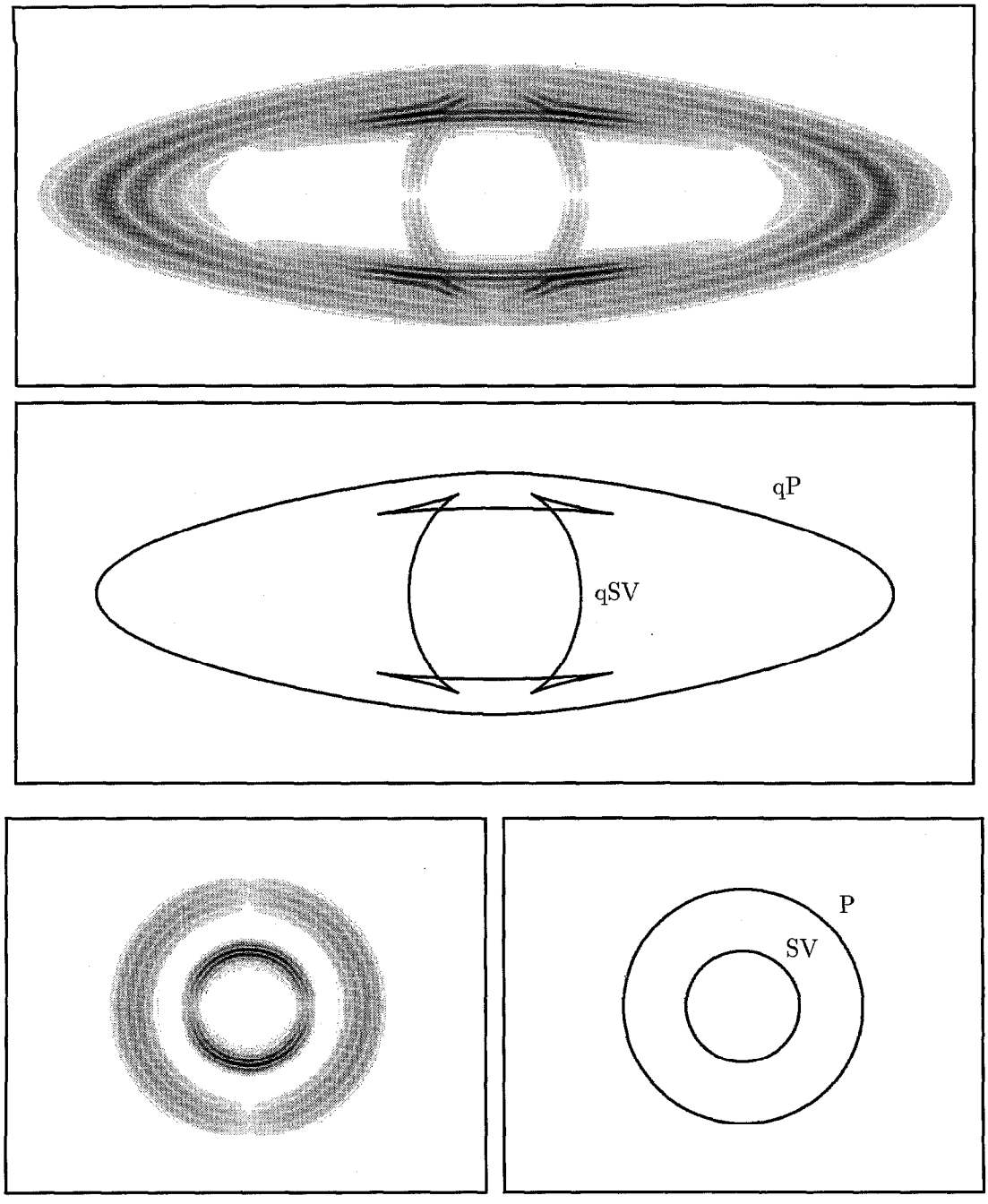

Fig. 3. Line force radiation into a transversely isotropic homogeneous medium ($\underline{\mathbf{a}}$ horizontally oriented, force parallel to $\underline{\mathbf{a}}$, Graphite-Epoxy 1 with $c_{11} = 145.8$, $c_{22} = 13.5$, $c_{44} = 3.4$, $c_{55} = 6.8$, $c_{12} = 10.2$ in GPa and $\varrho_0 = 1600\ \mathrm{kg/m^3}$): EFIT-$|\underline{\mathbf{v}}|$-snap-shot of the quasi-pressure (qP) and quasi-shear vertical (qSV) wavefronts and the group velocity diagrams compared to the isotropic homogeneous medium with pressure (P) and shear vertical (SV) wave

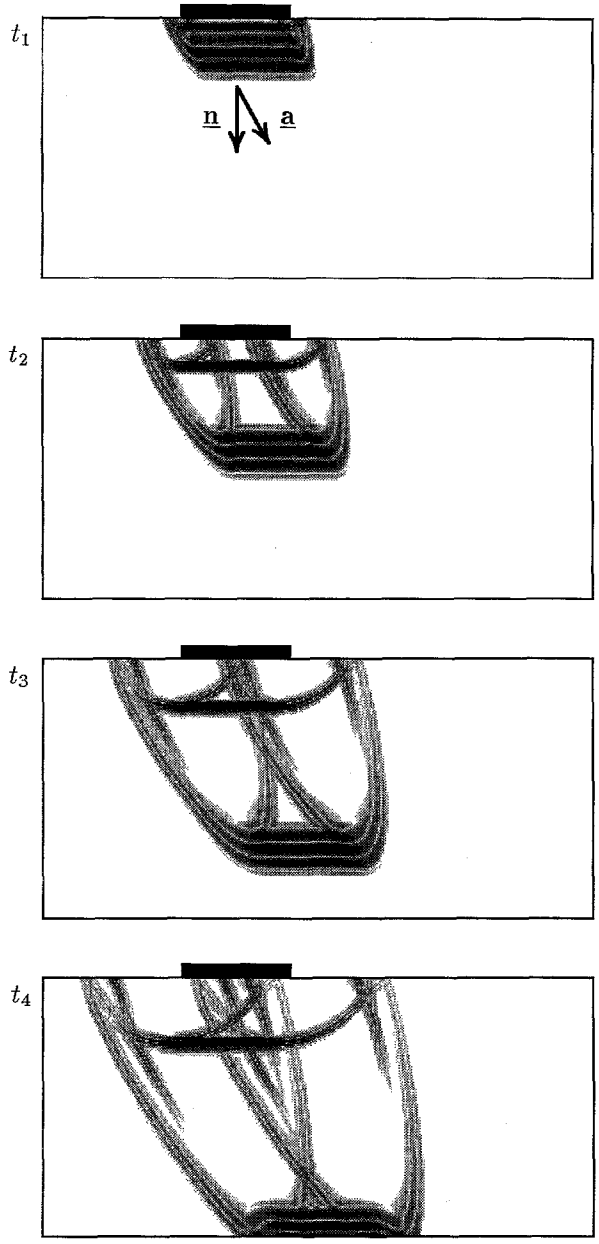

Fig. 4. Finite aperture radiation into transversely isotropic medium with **a** making an angle of 30° with regard to surface normal **n**; elastic material same as in Fig. 3: EFIT-|**v**|-snap-shots of quasi-pressure (qP), quasi-shear vertical (qSV) and pseudo surface waves

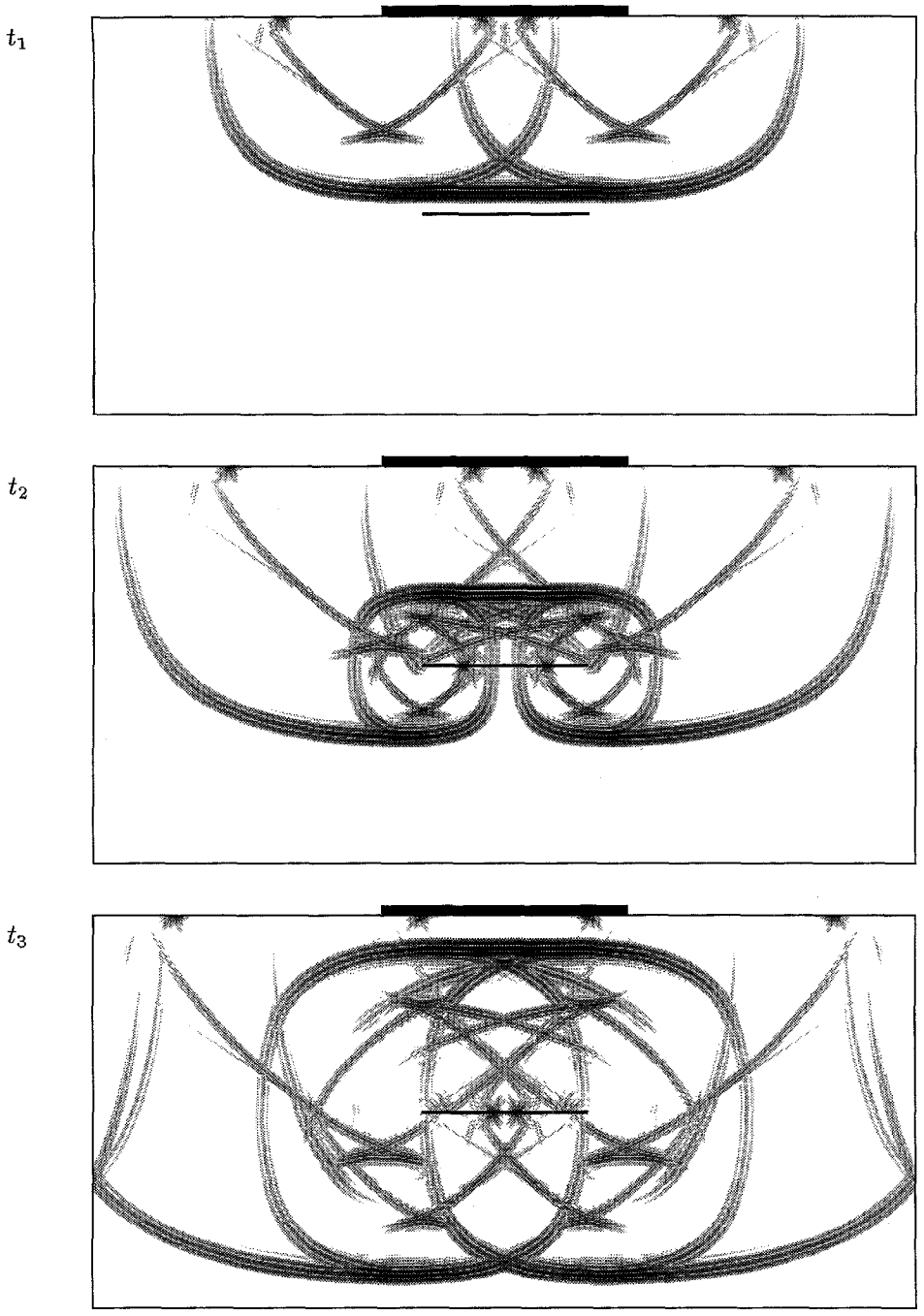

Fig. 5. Finite aperture radiation and crack scattering (stress-free boundary condition) in transversely isotropic homogeneous medium (a horizontally oriented; Austenite with $c_{11} = 236.6$, $c_{12} = 102.7$, $c_{22} = 262.5$, $c_{44} = 92.8$, $c_{55} = 118.7$ in GPa and $\varrho_0 = 8100$ kg/m^3)

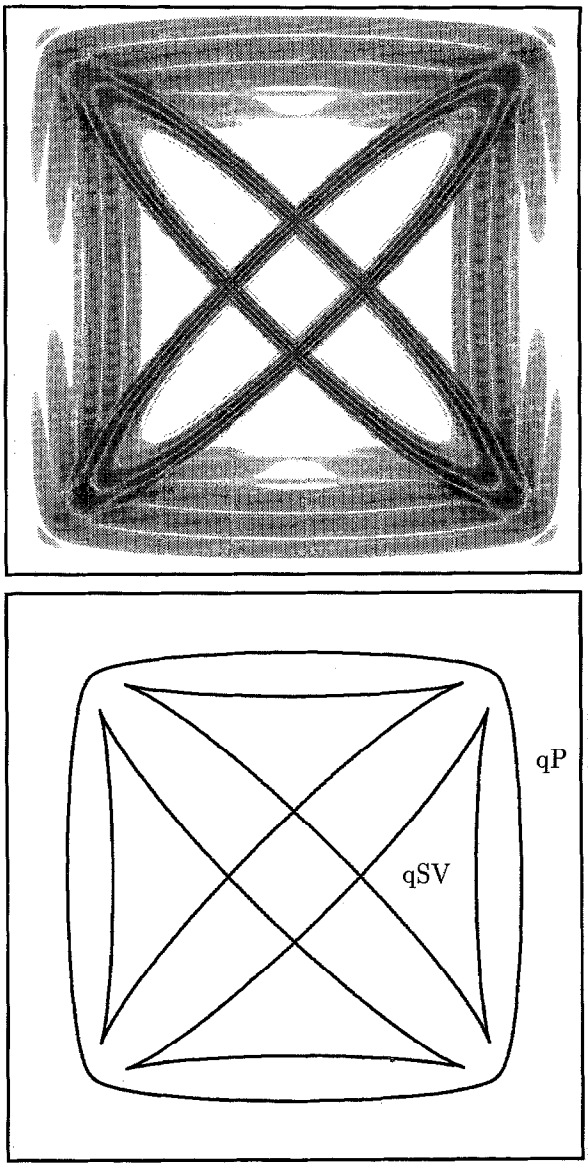

Fig. 6. Line force radiation into transversely isotropic homogeneous medium ($\underline{\mathbf{a}}$ and force horizontally oriented; $c_{11}/c_{55} = 0.64$, $c_{12}/c_{55} = 0.5523$, $c_{22}/c_{55} = 0.64$, $c_{44}/c_{55} = 0.04385$): EFIT-$|\underline{\mathbf{v}}|$-snap-shot of the quasi-pressure (qP) and quasi-shear vertical (qSV) wavefronts and the group velocity diagrams as compared to the EFIT wavefronts

where $c_{11}, c_{12}, c_{22}, c_{44}$, and c_{55} are five independent elastic constants replacing the Lamé's constants λ and μ of the isotropic case [3]; $\underline{\mathbf{a}}$ denotes the unit-vector perpendicular to which isotropy holds.

For crystals with cubic symmetry, $\underline{\underline{\underline{\mathbf{c}}}}$ has the representation

[3] The c's are the stiffness matrix elements in Voigt's notation for $\underline{\mathbf{a}}$ in x_1-direction with the hexagonal symmetry condition $c_{23} = c_{22} - 2c_{44}$. In [25,26] an alternative notation with the five elastic constants $\lambda_{\|}, \lambda_{\perp}, \mu_{\|}, \mu_{\perp}$, and ν is used. These are according to the c's as: $c_{11} = \lambda_{\|} + 2\mu_{\|}$, $c_{12} = \nu$, $c_{22} = \lambda_{\perp} + 2\mu_{\perp}$, $c_{44} = \mu_{\perp}$, $c_{55} = \mu_{\|}$ and $c_{23} = c_{22} - 2c_{44} = \lambda_{\perp}$.

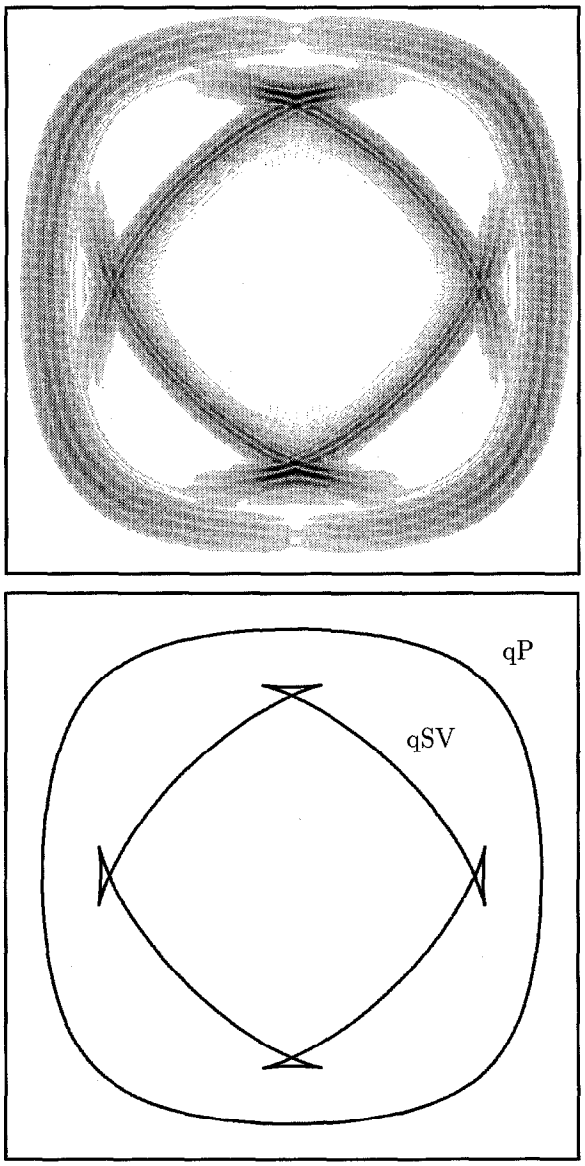

Fig. 7. Line force radiation into anisotropic medium with cubic symmetry; $\underline{\mathbf{m}}_i$ in x_i-direction; with $c_{11} = 106.9$, $c_{12} = 28.5$, $c_{44} = 62.6$ in GPa and $\varrho_0 = 2700$ kg/m^3: EFIT-$|\underline{\mathbf{v}}|$-snap-shot of the quasi-pressure (qP) and quasi-shear vertical (qSV) wavefronts and the group velocity diagrams as compared to the EFIT wavefronts

$$\underline{\underline{\underline{\underline{\mathbf{c}}}}}^{\mathrm{C}} = c_{12}\underline{\underline{\mathbf{I}}}\,\underline{\underline{\mathbf{I}}} + c_{44}\left(\underline{\underline{\mathbf{I}}}\,\underline{\underline{\mathbf{I}}}^{1324} + \underline{\underline{\mathbf{I}}}\,\underline{\underline{\mathbf{I}}}^{1342}\right) + (c_{11} - c_{12} - 2c_{44})\sum_{i=1}^{3}\underline{\mathbf{m}}_i\,\underline{\mathbf{m}}_i\,\underline{\mathbf{m}}_i\,\underline{\mathbf{m}}_i, \tag{A.6}$$

with three independent constants c_{11}, c_{12}, c_{44} and the cubic symmetry planes normal unit-vectors $\underline{\mathbf{m}}_i$ [4]. In case (A.5), the wave tensor adopts the form

[4] The c's are Voigt-notation matrix elements for $\underline{\mathbf{m}}_i$ in x_i-direction.

$$\underline{\underline{\mathbf{W}}}^{\mathrm{TI}}(\underline{\mathbf{K}},\omega) = \left[c_{44}K^2 + (c_{55}-c_{44})(\underline{\mathbf{a}}\cdot\underline{\mathbf{K}})^2 - \varrho_0\omega^2\right]\underline{\underline{\mathbf{I}}} + (c_{22}-c_{44})\underline{\mathbf{K}}\,\underline{\mathbf{K}} + \\ + \left\{\left[c_{11}+c_{22}-2(c_{12}+2c_{55})\right](\underline{\mathbf{a}}\cdot\underline{\mathbf{K}})^2 + (c_{55}-c_{44})K^2\right\}\underline{\mathbf{a}}\,\underline{\mathbf{a}} + \\ + \left[c_{12}+c_{55}-(c_{22}-c_{44})\right](\underline{\mathbf{a}}\cdot\underline{\mathbf{K}})(\underline{\mathbf{K}}\,\underline{\mathbf{a}}+\underline{\mathbf{a}}\,\underline{\mathbf{K}}), \tag{A.7}$$

with $K^2 = \underline{\mathbf{K}}\cdot\underline{\mathbf{K}}$, or, in short-hand notation

$$\underline{\underline{\mathbf{W}}}^{\mathrm{TI}}(\underline{\mathbf{K}},\omega) = \alpha\underline{\underline{\mathbf{I}}} + \beta\underline{\mathbf{K}}\,\underline{\mathbf{K}} + \gamma\underline{\mathbf{a}}\,\underline{\mathbf{a}} + \delta\underline{\mathbf{K}}\,\underline{\mathbf{a}} + \varepsilon\underline{\mathbf{a}}\,\underline{\mathbf{K}}, \tag{A.8}$$

with $\delta = \varepsilon$. Similarly, we obtain for case (A.6)

$$\underline{\underline{\mathbf{W}}}^{\mathrm{C}}(\underline{\mathbf{K}},\omega) = \left(c_{44}K^2 - \varrho_0\omega^2\right)\underline{\underline{\mathbf{I}}} + (c_{12}+c_{44})\underline{\mathbf{K}}\,\underline{\mathbf{K}} + (c_{11}-c_{12}-2c_{44})\sum_{i=1}^{3}(\underline{\mathbf{m}}_i\cdot\underline{\mathbf{K}})^2\underline{\mathbf{m}}_i\,\underline{\mathbf{m}}_i, \tag{A.9}$$

or, in short-hand notation

$$\underline{\underline{\mathbf{W}}}^{\mathrm{C}}(\underline{\mathbf{K}},\omega) = \alpha\underline{\underline{\mathbf{I}}} + \beta\underline{\mathbf{K}}\,\underline{\mathbf{K}} + \gamma\underline{\mathbf{m}}_1\,\underline{\mathbf{m}}_1 + \delta\underline{\mathbf{m}}_2\,\underline{\mathbf{m}}_2 + \varepsilon\underline{\mathbf{m}}_3\,\underline{\mathbf{m}}_3, \tag{A.10}$$

with, of course, different meaning of the coefficients $\alpha,\beta,\gamma,\delta,\varepsilon$.

Equating the determinant of the wave tensor to zero results in a polynominal in K, its zeros determining the wave numbers of possible plane wave solutions of (A.1) with propagation directions prescribed by the components of the unit-vector $\hat{\underline{\mathbf{K}}} = \underline{\mathbf{K}}/K$. That way, the directional dependence of the phase velocity or slowness is obtained.

Applying dyadic algebra [24] to (A.8) yields

$$\det\underline{\underline{\mathbf{W}}}^{\mathrm{TI}}(\underline{\mathbf{K}},\omega) = \alpha\left\{\alpha^2 + \alpha\left(\beta K^2 + \gamma + 2\varepsilon\underline{\mathbf{a}}\cdot\underline{\mathbf{K}}\right) + \left(\beta\gamma - \varepsilon^2\right)\left[K^2 - (\underline{\mathbf{a}}\cdot\underline{\mathbf{K}})^2\right]\right\}, \tag{A.11}$$

and, respectively

$$\det\underline{\underline{\mathbf{W}}}^{\mathrm{C}}(\underline{\mathbf{K}},\omega) \\ = \alpha^3 + \alpha^2(\beta K^2 + \gamma + \delta + \varepsilon) \\ + \alpha\left\{\beta K^2(\gamma+\delta+\varepsilon) + \delta\varepsilon + \gamma\varepsilon + \gamma\delta) - \right. \\ \left. - \beta K^2\left[\gamma(\underline{\mathbf{m}}_1\cdot\underline{\mathbf{K}})^2 + \delta(\underline{\mathbf{m}}_2\cdot\underline{\mathbf{K}})^2 + \varepsilon(\underline{\mathbf{m}}_3\cdot\underline{\mathbf{K}})^2\right]\right\} \\ + \beta K^2\left[\delta\varepsilon(\underline{\mathbf{m}}_1\cdot\underline{\mathbf{K}})^2 + \gamma\varepsilon(\underline{\mathbf{m}}_2\cdot\underline{\mathbf{K}})^2 + \gamma\delta(\underline{\mathbf{m}}_3\cdot\underline{\mathbf{K}})^2\right] + \gamma\delta\varepsilon\,. \tag{A.12}$$

Inserting $\alpha,\beta,\gamma,\varepsilon$ into (A.11) reveals a factorization of the slowness polynominal allowing for its analytical solution [25,26] in terms of two quasi-shear wave modes and one quasi-pressure wave mode. Therefore, the directional dependence of the group velocity $\underline{\mathbf{c}}_g$ as defined by

$$\underline{\mathbf{c}}_{g\eta} = \left(\frac{\partial\omega(\underline{\mathbf{K}})}{\partial\underline{\mathbf{K}}}\right)_{\underline{\mathbf{K}}=\underline{\mathbf{K}}_\eta}, \tag{A.13}$$

where η denotes the wave mode under concern, can also be computed analytically. Unfortunately, this factorization does not appear in $\det\underline{\underline{\mathbf{W}}}^{\mathrm{C}}$, so standard numerical techniques (Cardan's formulas) have to be utilized for computation of slowness and group velocity surfaces in 3D. A factorization is only observed in 2D. If we only consider two-dimensional elastic wave propagation, where the wave vector $\underline{\mathbf{K}}$ is coplanar with $\underline{\mathbf{a}}$ in the "TI"-case and perpendicular to one $\underline{\mathbf{m}}_i$ in the "C"-case respectively, one quasi-shear mode separates. The remaining two wave modes – one quasi-shear and one quasi-pressure – are coupled via excitation, boundaries, interfaces and scattering surface as shown in our numerical results of Figs. 3-7.

Exploiting the above procedure yields the group velocity curves of Figs. 3, 6 and 7.

References

[1] J.D. Achenbach, A.K. Gautesen, H. McMaken, *Ray Methods for Waves in Elastic Solids*, Pitman, Boston (1982).

[2] Y.H. Pao, V. Varatharajulu, "Huygens' Principle, Radiation Conditions, and Integral Formulas for the Scattering of Elastic Waves", *J. Acoust. Soc. Am. 59*, 6, 1361-1371 (1976).

[3] L.J. Bond, M. Punjani, N. Saffari, "Ultrasonic Wave Propagation and Scattering Using Explicit Finite Difference Methods", in: M. Blakemore, G.A. Georgiou, eds., *Mathematical Modelling in Non-Destructive Testing*, Clarendon Press, Oxford (1988) 81-124.

[4] J. Virieux, "P-SV Wave Propagation in Heterogeneous Media: Velocity-Stress Finite-Difference Method", *Geophysics 51*, 4, 889-901 (1986).

[5] R. Ludwig, W. Lord, "A Finite-Element Formulation for the Study of Ultrasonic NDT Systems", *IEEE Trans. Ultrasonics, Ferroelectrics, and Frequency Control 35*, 6, 809-820 (1988).

[6] P. Fellinger, K.J. Langenberg, "Numerical Techniques for Elastic Wave Propagation and Scattering", in: S.K. Datta, J.D. Achenbach, Y.S. Rajapakse, eds., *Elastic Waves Ultrasonic Nondestructive Evaluation*, North-Holland, Amsterdam (1990) 81-86.

[7] P. Fellinger, Ein Verfahren zur numerischen Lösung elastischer Wellenausbreitungsprobleme im Zeitbereich durch direkte Diskretisierung der elastodynamischen Grundgleichungen, Ph.D. Thesis, Dept. of Electrical Engineering, University of Kassel, Kassel/Germany (1989).

[8] M. Bartsch et al., "Solution of Maxwell's Equations", *Computer Physics Communications 72*, 22-39 (1992).

[9] R. Marklein, P. Fellinger, K.J. Langenberg, "Die US-Modellierungcodes AFIT und EFIT als Werkzeuge zur quantitativen Fehlerbewertung", in: *Vorträge und Plakatberichte DGZfP-Jahrestagung 1992 Zerstörungsfreie Materialprüfung*, Berichtsband 33, Teil 2, BAM, Berlin (1992) 823-833.

[10] K.J. Langenberg, P. Fellinger, R. Marklein, P. Zanger, K. Mayer, T. Kreutter, "Inverse Methods and Imaging", in: J.D. Achenbach, ed., *Evaluation of Materials and Structures by Quantitative Ultrasonics*, Springer-Verlag, Vienna (1993) 317-398.

[11] J. Miklowitz, *The Theory of Elastic Waves and Waveguides*, North-Holland, Amsterdam (1978).

[12] J.D. Achenbach, *Wave Propagation in Elastic Solids*, North-Holland, Amsterdam (1973).

[13] B.A. Auld, *Acoustic Fields and Waves in Solids*, Robert E. Krieger Publ. Comp., Malabar, Florida (1990).

[14] A. Ben-Menahem, S.J. Singh, *Seismic Waves and Sources*, Springer-Verlag, New York (1981).

[15] K.J. Langenberg, P. Fellinger, R. Marklein, "On the Nature of the So-Called Subsurface Longitudinal and/or the Surface Longitudinal Creeping Wave", *Res. Nondestr. Testing 2*, 2, 59-81 (1990).

[16] R. Marklein, Die Akustische-Finite-Integrations-Technik (AFIT) – Ein numerisches Verfahren zur Lösung von Problemen der Abstrahlung, Ausbreitung und Streuung von akustischen Wellen im Zeitbereich, Master Thesis, Dept. of Electrical Engineering, University of Kassel, Kassel/Germany (1992).

[17] R. Marklein, Ein Vergleich zwischen der Methode der Finiten Elemente und der Technik der Finiten Integration zur numerischen Lösung von Problemen der elastischen Wellenausbreitung im Zeitbereich, Report, Dept. of Electrical Engineering, University of Kassel, Kassel/Germany (1991).

[18] R.D. Richtmyer, K.W. Morton, *Difference Methods for Initial Value Problems*. Wiley, New York (1967).

[19] A. Taflove, M.E. Brodwin, "Numerical Solution of Steady-State Electromagnetic Scattering Problems Using the Time-Dependent Maxwell's Equations", *IEEE Trans. Microwave Theory and Techniques 23*, 8, 623-630 (1975).

[20] R. Courant, K. Friedrichs, H. Lewy, "Über die partiellen Differenzengleichungen der mathematischen Physik", *Mathematische Annalen 100*, 32-74 (1928).

[21] John C. Strikwerda, *Finite Difference Schemes and Partial Differential Equations*, Wadsworth & Brooks/Cole, Mathematics Series, Pacific Grove, California (1989).

[22] C.-Y. Wang, J.D. Achenbach, "A New Look at 2-D Time-Domain Elastodynamic Green's Functions for General Anisotropic Solids", *Wave Motion 16*, 4, 389-405 (1992).

[23] J.H.M.T. van der Hijden, *Propagation of Transient Elastic Waves in Stratified Anisotropic Media*, North-Holland, Amsterdam (1987).

[24] H.C. Chen, *Theory of Electromagnetic Waves*, McGraw-Hill, New York (1983).

[25] M. Spies, *Elastische Wellen in transversal-isotropen Medien: ebene Wellen, Gaußsche Wellenpakete, Greensche Funktionen, elastische Holographie*, Ph.D. Thesis, University of Saarbrücken, Saarbrücken/Germany (1992).

[26] M. Spies, P. Fellinger, K.J. Langenberg, "Elastic Waves in Homogeneous and Layered Transversely Isotropic Media: Gaussian Wave Packets and Green Functions", in: D.O. Thompson, D.E. Chimenti, eds., *Review of Progress in Quantitative Nondestructive Evaluation 12*, Plenum Press, New York (1992) 123-130.